Loss of AMP-Activated Protein Kinase-α2 Impairs the Insulin-Sensitizing Effect of Calorie Restriction in Skeletal Muscle

Pei Wang,[1] Ruo-Yu Zhang,[1] Jie Song,[1] Yun-Feng Guan,[1] Tian-Ying Xu,[1] Hui Du,[1] Benoit Viollet,[2,3] and Chao-Yu Miao[1]

Whether the well-known metabolic switch AMP-activated protein kinase (AMPK) is involved in the insulin-sensitizing effect of calorie restriction (CR) is unclear. In this study, we investigated the role of AMPK in the insulin-sensitizing effect of CR in skeletal muscle. Wild-type (WT) and AMPK-α2$^{-/-}$ mice received ad libitum (AL) or CR (8 weeks at 60% of AL) feeding. CR increased the protein level of AMPK-α2 and phosphorylation of AMPK-α2. In WT and AMPK-α2$^{-/-}$ mice, CR induced comparable changes of body weight, fat pad weight, serum triglycerides, serum nonesterified fatty acids, and serum leptin levels. However, decreasing levels of fasting/fed insulin and fed glucose were observed in WT mice but not in AMPK-α2$^{-/-}$ mice. Moreover, CR-induced improvements of whole-body insulin sensitivity (evidenced by glucose tolerance test/insulin tolerance test assays) and glucose uptake in skeletal muscle tissues were abolished in AMPK-α2$^{-/-}$ mice. Furthermore, CR-induced activation of Akt-TBC1D1/TBC1D4 signaling, inhibition of mammalian target of rapamycin−S6K1−insulin receptor substrate-1 pathway, and induction of nicotinamide phosphoribosyltransferase−NAD$^+$−sirtuin-1 cascade were remarkably impaired in AMPK-α2$^{-/-}$ mice. CR serum increased stability of AMPK-α2 protein via inhibiting the X chromosome-linked ubiquitin-specific protease 9–mediated ubiquitylation of AMPK-α2. Our results suggest that AMPK may be modulated by CR in a ubiquitylation-dependent manner and acts as a chief dictator for the insulin-sensitizing effects of CR in skeletal muscle. ***Diabetes*** **61:1051–1061, 2012**

Calorie restriction (CR) with adequate nutrition has been shown to improve age-related diseases and to slow the aging process (1). Moreover, CR results in weight loss and improvement for metabolic disorders (2–4). Many experimental and clinical studies show that insulin sensitivity is significantly improved by CR (5–7). CR could modulate insulin receptor (IR)/insulin-like growth factor I (IGF-I) receptor (IGF-IR) signaling (i.e., serum insulin/IGF-I levels) (8), IR substrate (IRS)-1 phosphorylation (9), and IRS-associated PI 3-kinase−Akt activity (10).

The AMP-activated protein kinase (AMPK) is a member of the SNF1/AMPK protein kinase family and serves as an energy sensor in all eukaryotic cells (11,12). It consists of one catalytic subunit (α) and two regulatory subunits (β and γ) (11,12). Upon activation by AMP (11,12) and ADP (13), AMPK shuts down anabolic pathways, such as synthesis of fatty acid, triglyceride, and cholesterol as well as transcriptional processes, and promotes catabolic pathways. AMPK has been shown to influence insulin sensitivity under both normal and high-fat diet (14–16) and can be activated by CR (17,18). The metabolic effects of resveratrol, a well-known CR mimetic compound, recently were found to require AMPK (14). On the basis of the findings summarized above, we speculate that CR could improve insulin sensitivity by activating AMPK. Moreover, in a very recent review, Cantó and Auwerx (19) proposed that AMPK is a key sensor or effector in CR-induced beneficial effects.

Here, we demonstrate that AMPK is a primary sensor that controls insulin sensitivity upon CR in skeletal muscle through regulating phosphorylation of the mammalian target of rapamycin (mTOR)−S6K1−IRS-1 signaling pathway and activation of the nicotinamide phosphoribosyltransferase (Nampt)-sirtuin (SIRT1) axis.

RESEARCH DESIGN AND METHODS

Agents. Antibodies against total AMPK, phospho-AMPK^{Thr172} (2535), phospho-Tyr (9411), phospho-Thr (9381), phospho–IR-β (Tyr$^{1150/1151}$) (3024), phospho–IRS-1^{Ser1101} (2385), phospho–IRS-1$^{Ser636/639}$ (2388), phospho–IRS-1^{Ser602} (2386), phospho–IRS-1^{Ser307} (2381), phospho-mTOR^{Ser2448} (2971), total-mTOR (2983), phospho-mTOR^{Ser2448} (2971), phospho-S6K1^{Ser389} (9205), and total–IRS-1 were purchased from Cell Signaling Technology (Danvers, MA). Antibodies against AMPK-α2, Nampt, peroxisome proliferator–activated receptor γ coactivator (PGC)-1α, and forkhead box class O (FOXO)1 were from Santa Cruz Biotechnology (Santa Cruz, CA). Anti-SIRT1 was from Upstate Biotechnology (Charlottesville, VA). Anti-acetylated Lys (4G12) was from Millipore (Bedford, MA).

Animals and caloric restriction. Male C57BL/6J mice were purchased from Sino-British SIPPR/BK Laboratory Animal Ltd. (Shanghai, China). AMPK-α2$^{-/-}$ mice and their corresponding wild-type (WT) mice were bred as described previously (16,20). During the experiments, mice were housed in a facility with controlled temperature (23–25°C) and lighting (0800 to 2000 h), with free access to tap water. All procedures were performed in compliance with relevant institutional guidelines for animal care.

CR started at age 8–10 weeks and lasted for 8 weeks (four mice per cage). In the CR group, food was adjusted on a daily basis to 60% of the amount consumed by free-feeding mice (the ad libitum [AL] group) for a duration of 2 months. The standard chow for mice was purchased from Sino-British SIPPR/BK Laboratory Animal Ltd. This diet contains 20% protein, 5% fat, and a variety of essential vitamins and trace elements.

Glucose tolerance test and insulin tolerance test. Mice underwent overnight fasting before glucose tolerance test (GTT) and insulin tolerance test (ITT). For GTT, mice received intraperitoneal injection of glucose (2 g/kg body wt). Blood samples were collected from the tail vein at 0, 15, 30, 60, and 120 min. Blood insulin levels were determined by ELISA (Linco, St. Charles, MO). For ITT, mice received intraperitoneal injection of insulin (2.0 units/kg). Blood samples were taken at 0, 15, 30, 60, 90, and 120 min. Blood glucose concentration was determined using whole blood with an automatic glucose monitor (One-Touch Ultra, LifeScan; Johnson & Johnson, Milpitas, CA).

From the [1]Department of Pharmacology, Second Military Medical University, Shanghai, China; the [2]Institut Cochin, Université Paris Descartes, Centre National de la Recherche Scientifique (Unité Mixte de Recherche 8104), Paris, France; and [3]INSERM U1016, Paris, France.

Corresponding author: Chao-Yu Miao, cymiao@smmu.edu.cn, or Pei Wang, pwang@smmu.edu.cn.

Received 23 August 2011 and accepted 18 January 2012.

DOI: 10.2337/db11-1180

This article contains Supplementary Data online at http://diabetes.diabetesjournals.org/lookup/suppl/doi:10.2337/db11-1180/-/DC1.

© 2012 by the American Diabetes Association. Readers may use this article as long as the work is properly cited, the use is educational and not for profit, and the work is not altered. See http://creativecommons.org/licenses/by-nc-nd/3.0/ for details.

Measurement of metabolic parameters. Body weight was recorded every week. At the end of CR treatment, mice were anesthetized with phenobarbital sodium (35 mg/kg) and epididymal fat was isolated and weighed. Blood was collected from the heart and allowed to clot and then centrifuged for 20 min at 2,500 rpm to obtain serum. The nonesterified fatty acid (NEFA) concentration in serum was measured with the use of a NEFA-C test (Wako, Osaka, Japan). Serum adiponectin and leptin levels were measured with ELISA kits (R&D Systems, Minneapolis, MN). Serum insulin concentration was determined by ELISA (Linco). Serum lipid and glucose levels were measured using a Beckman biomedical autoanalyzer (Beckman Instruments, Bream, CA).

Glucose uptake in skeletal muscle tissue. Glucose uptake was measured using a nonradioactive fluorescent glucose [2-(*N*-(7-nitrobenz-2-oxa-1,3-diazol-4-yl)amino)-2-deoxyglucose] (2-NBDG) method, as described previously (21). Extensor digitorum longus skeletal muscle isolated from WT and AMPK-$\alpha2^{-/-}$ mice was incubated at 37°C for 30 min in oxygenated (95% O_2 + 5% CO_2) Krebs-Henseleit buffer containing 0.5% BSA, 2 mmol/L sodium pyruvate, and 6 mmol/L mannitol for 10 min prior to 30-min insulin exposure (0.8 mmol/L) followed by 15-min 2-NBDG (50 μmol/L) incubation. The specimens were blotted up on filter paper, trimmed, and extracted using a lysis buffer. The amount of 2-NBDG in skeletal muscle was determined using a microplate fluorimeter (Infinite M200; Tecan, Hillsborough, NC) as previously described (22).

Cell culture and transfection. Mouse C2C12 myoblasts were purchased from American Type Culture Collection and cultured with Dulbecco's modified Eagle's medium supplemented with 10% (v/v) FBS, 2 mmol/L glutamate, 15 mmol/L HEPES, 500 IU/mL penicillin, and 100 μg/mL streptomycin in 95% O_2 and 5% CO_2. To obtain fully differentiated myotubes, FBS was removed from cell culture at 70% confluence. Cells were incubated in a medium containing only 2% (v/v) horse serum for 4 additional days. Transfection of small interfering (si)RNA was performed as described previously (23) using Lipofectamine 2000 (Invitrogen, Carlsbad, CA). siRNAs targeting X chromosome-linked ubiquitin-specific protease (USP)-9 (USP9X), USP5, and USP7 were purchased from Santa Cruz Biotechnology. Flow cytometry revealed 70–80% transfection efficiency.

Immunoblotting. Immunoblotting analyses on extracts of skeletal muscle or cell extracts were performed using Odyssey Infrared Fluorescence Imaging System (LI-COR Biosciences, Lincoln, NE) as described previously (20,24). Samples were homogenized with a lysis buffer (Pierce, Rockford, IL) containing a protease inhibitor cocktail (Pierce). Samples were subjected to 10–12% SDS-PAGE, electrotransferred to nitrocellulose membranes, probed with a primary antibody overnight, and then incubated with an appropriate secondary antibody conjugated with infrared dyes 800 and 680 (LI-COR Biosciences). All immunoblotting experiments were repeated at least three times.

Immunoprecipitation. Immunoprecipitation experiments were performed as described previously (20). In brief, tissues or cells were homogenated with radioimmunoprecipitation assay buffer containing a protease inhibitor cocktail (Pierce). To reduce nonspecific binding, we added 50 μL normal rabbit serum to 1 mL homogenate and incubated for 1 h on ice. Protein bead A/G (100 μL; Santa Cruz Biotechnology) was then added to the homogenate and incubated for 1 h with gentle agitation. The supernatant was incubated with a primary antibody at 4°C overnight. Protein A/G agarose was used to harvest the antigen-antibody complex. The samples were separated on 10% SDS-PAGE pages for immunoblotting.

Quantitative PCR. Total RNA was extracted using Trizol (Invitrogen). cDNAs were generated by Maloney murine leukemia virus reverse transcription (Promega, Madison, WI) and analyzed by quantitative PCR with a SYBR green PCR kit (Takara, Otsu, Japan) and Opticon Monitor 3 Real-time PCR system (Bio-Rad, Hercules, CA). All data were normalized to β-actin expression ($2^{-\triangle\triangle}$ cycle threshold method) (25). Primers are listed in Supplementary Table 1.

Measurements of NAD^+ and SIRT1 activity. The assays for NAD^+ level and SIRT1 activity were performed as described previously (20). NAD^+ levels were determined with a NAD^+ quantification kit (BioVision, Mountain View, CA). To evaluate the SIRT1 activity, tissue was extracted using a mild lysis buffer plus protease inhibitor mix. SIRT1 was enriched by immunoprecipitation using a monoclonal anti-SIRT1 antibody (Santa Cruz Biotechnology). SIRT1 activity was examined using deacetylation assay with the Fluorimetric Drug Discovery Kit (AK-555; Biomol, Plymouth, PA) as described previously (20).

Cells treated with CR serum. This experiment was performed as described previously (26). In brief, all serum was obtained from fasted, anesthetized AL or CR C57BL/J6 mice. After 8 weeks of AL or CR treatment, mice were anesthetized and a catheter was inserted into the left carotid artery. A total of 1 mL whole blood was collected and allowed to clot (30 min) and then centrifuged for 20 min at 2,500 rpm. The serum samples were heat inactivated at 56°C for 30 min before use in cell culture experiments. Cells were serum starved for 6 h and then treated with AL or CR serum (final concentration: 10%) for 8 h.

Determination of degradation of AMPK-α2 protein. C2C12 myoblasts were seeded in a 6-well plate and differentiated into myotubes. Myotubes were serum starved for 6 h and then exposed to AL or CR serum plus 150 μg/mL cycloheximide (CHX). Cells were harvested at different time points after CHX treatment, and cell extracts were immunoblotted with an anti–AMPK-α2 or anti-actin antibody.

Phosphatase activity assay. Protein phosphatase (PP)2A and PP2C activity was determined using a nonradioactive Ser/Thr phosphatase activity assay (Promega) as reported previously (27). In brief, cell lysate was incubated with 10 μg monoclonal PP2A antibody (Upstate Biotech, Lake Placid, NY) at 4°C overnight. Protein A/G plus agarose was added and allowed to form a complex for 4 h at 4°C. Immunocomplexes were washed three times with washing buffer. Phosphatase activity was assayed by suspending the final pellet in 15 mL buffer containing 1 mmol/L phosphopeptide substrate RRA(pT)VA for 20 min at 25°C. The reaction was stopped by the addition of 50 μL molybdate dye solution, and the phosphatase activity was read at 600 nm in a fluorimeter (Tecan).

Statistical analysis. Data are expressed as mean ± SEM. Differences were evaluated by two-tailed Student *t* test or ANOVA followed by Tukey post hoc test. Statistical significance was set at $P < 0.05$.

RESULTS

CR activates AMPK signaling pathway and increases the protein level of AMPK-α2. At first, we studied the activation of AMPK signaling pathway during CR. CR activated AMPK signaling pathway in skeletal muscle (Fig. 1*A*), evidenced by enhanced phosphorylation of Thr^{172} of AMPK-α2 and phosphorylation of acetyl CoA carboxylase (ACC), a downstream target of AMPK (Fig. 1*B*).

Quantitative PCR revealed higher mRNA level of the AMPK-α2 subunit (>10-fold vs. AMPK-α1 subunit) (Supplementary Fig. 1*A*) in mouse skeletal muscle. CR increased AMPK-α2 protein (Fig. 1*C*) but not AMPK-α1 protein (Supplementary Fig. 1*B*). Thr phosphorylation of AMPK-α2 was also significantly increased by CR (Fig. 1*D*). On the basis of these findings, we focused on the role of AMPK-α2 in the CR-induced insulin-sensitizing effect in skeletal muscle in the next set of experiments.

Influence of AMPK-α2 knockout on whole-body characterizations in mice upon CR. After 8 weeks of AL and CR treatment, whole-body characterizations were monitored in WT and AMPK-$\alpha2^{-/-}$ mice. Body weight reduction induced by CR was comparable between WT and AMPK-$\alpha2^{-/-}$ mice (Table 1). Consistent changes were also observed in epididymal fat weight. It is interesting that CR induced a decrease of fasting/fed insulin levels in WT mice but not in AMPK-$\alpha2^{-/-}$ mice. CR reduced fed glucose levels in WT mice but not in AMPK-$\alpha2^{-/-}$ mice. CR induced a comparable decrease of serum triglyceride levels, enhancement of serum NEFAs, and decline of leptin levels in WT and AMPK-$\alpha2^{-/-}$ mice. CR did not affect serum adiponectin levels in either WT or AMPK-$\alpha2^{-/-}$ mice.

CR-induced increase of whole-body insulin sensitivity and enhancement of glucose uptake in skeletal muscle requires AMPK-α2. ITT assay revealed enhanced insulin sensitivity upon CR in WT mice (Fig. 2*A*) but not in AMPK-$\alpha2^{-/-}$ mice (Fig. 2*B*). In GTT assay, we observed a consistent effect (Fig. 2*C* and *D*). Next, we studied the effect of AMPK-α2 deletion on insulin-induced glucose uptake in isolated skeletal muscle. Under basal condition, there were no differences among the four groups (Fig. 2*E*). However, under insulin stimulation, CR significantly increased the glucose uptake in WT mouse skeletal muscle but not in AMPK-$\alpha2^{-/-}$ mouse skeletal muscle (Fig. 2*E*).

Loss of AMPK-α2 inhibits CR-induced IRS-1–Akt pathway activation. The disappearance of the insulin-sensitizing effect of CR in AMPK-$\alpha2^{-/-}$ mice raises the possibility that ablation of AMPK-α2 could impair the insulin-related signaling pathways. We examined the phosphorylation of IR/IGF-IR. CR enhanced phosphorylation of IR-β/IGF-IR-β

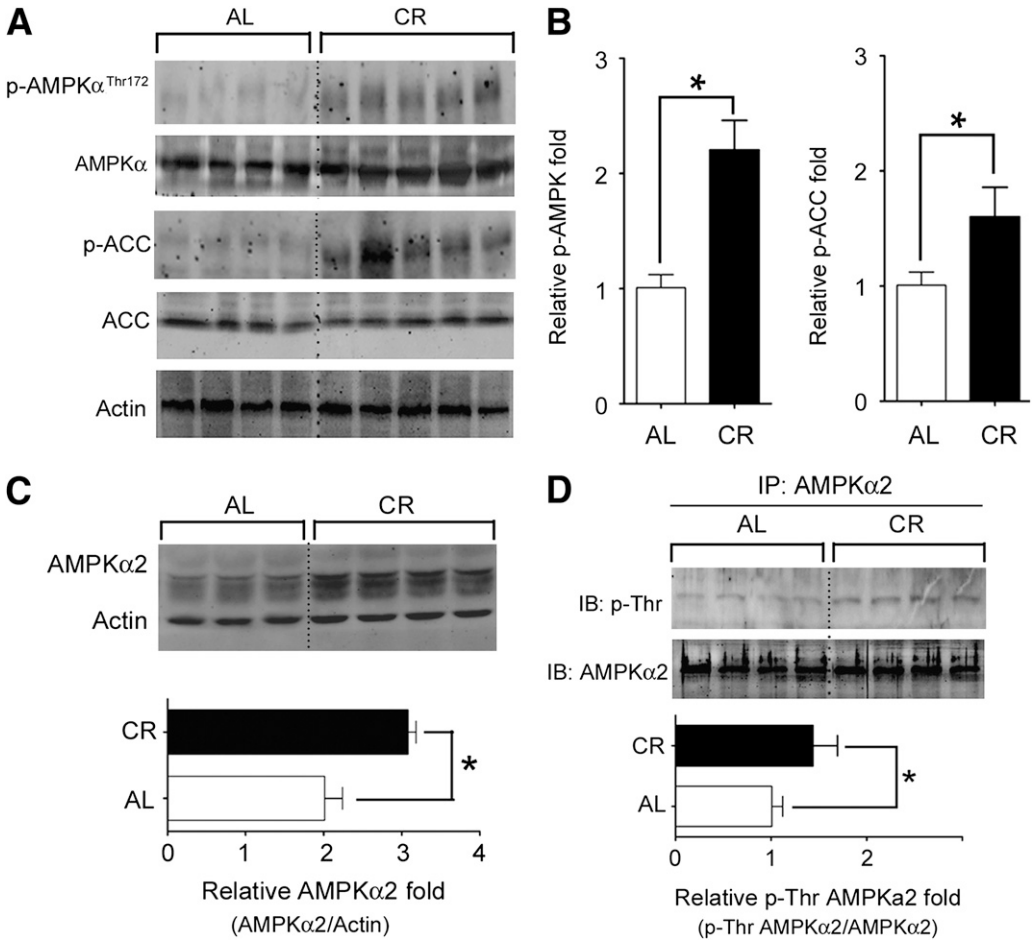

FIG. 1. CR increases the protein level of AMPK-α2 subunit and phosphorylation of AMPK-α2. *A* and *B*: CR for 8 weeks increased the phosphorylation of AMPK and ACC, an AMPK target in skeletal muscle. *C*: CR increased total AMPK-α2 protein level. *D*: AMPK-α2 in skeletal muscle lysate was enriched by immunoprecipitation and then probed with an anti–phospho-Thr antibody to detect the Thr phosphorylation of AMPK-α2. *P < 0.05 vs. AL. n = 4–6 per group. IP, immunoprecipitation; IB, immunoblot.

in WT mice in response to bolus insulin injection and produced comparable increase in IR-β/IGF-IR-β phosphorylation in AMPK-α2$^{-/-}$ mice (Supplementary Fig. 2).

We next tested the Tyr phosphorylation of IRS-1. Under basal condition, there was no apparent Tyr phosphorylation of IRS-1 (Fig. 3*A*). Under insulin stimulation, CR increased Tyr phosphorylation of IRS-1 in WT control mice but less so in AMPK-α2 knockout mice (Fig. 3*A*). CR-treated WT mice exhibited remarkable increase of phosphorylation of Akt (Fig. 3*B*), which was attenuated in AMPK-α2$^{-/-}$ mice (Fig. 3*B*).

TABLE 1
Effects of CR on body weight, epididymal fat pad weight, and serum parameters in WT vs. AMPK-α2$^{-/-}$ mice

	WT		AMPK-α2$^{-/-}$	
	AL	CR	AL	CR
Initial weight (g)	23.6 ± 1.2	24.3 ± 1.1	24.1 ± 2.1	24.3 ± 1.7
Final weight (g)	30.4 ± 2.1	21.8 ± 1.5*	31.7 ± 2.5	21.1 ± 1.8*
Weight gain (g)	6.8 ± 0.8	−2.5 ± 0.3*	7.3 ± 0.5	−2.2 ± 0.2*
Epididymal fat weight (g)	0.91 ± 0.35	0.06 ± 0.001*	1.16 ± 0.23	0.07 ± 0.001*
Serum metabolites				
Fasting insulin (ng/mL)	0.67 ± 0.08	0.52 ± 0.05*	0.64 ± 0.06	0.62 ± 0.09
Fed insulin (ng/mL)	1.36 ± 0.2	0.92 ± 0.15*	1.13 ± 0.13†	1.10 ± 0.17†
Fasting glucose (mmol/L)	6.2 ± 0.7	6.0 ± 0.4	6.9 ± 0.7	6.4 ± 0.6
Fed glucose (mmol/L)	9.2 ± 1.1	8.1 ± 1.0*	11.6 ± 1.6†	11.2 ± 1.6†
Triglycerides (mmol/L)	0.74 ± 0.14	0.49 ± 0.07*	0.81 ± 0.16	0.52 ± 0.15*
NEFAs (mEq/L)	0.41 ± 0.08	0.65 ± 0.09*	0.49 ± 0.11	0.71 ± 0.13*
Leptin (ng/mL)	0.71 ± 0.11	0.57 ± 0.07*	0.73 ± 0.081	0.61 ± 0.05*
Adiponectin (μg/mL)	7.8 ± 1.6	8.1 ± 2.1	7.5 ± 1.8	7.7 ± 2.3

Data are means ± SE and were analyzed with two-way ANOVA (genotype × diet) followed by Tukey post hoc analysis. CR lasted for 8 weeks. *P < 0.05 CR vs. AL within genotype. †P < 0.05 knockout vs. AL within diet. n = 8 per group.

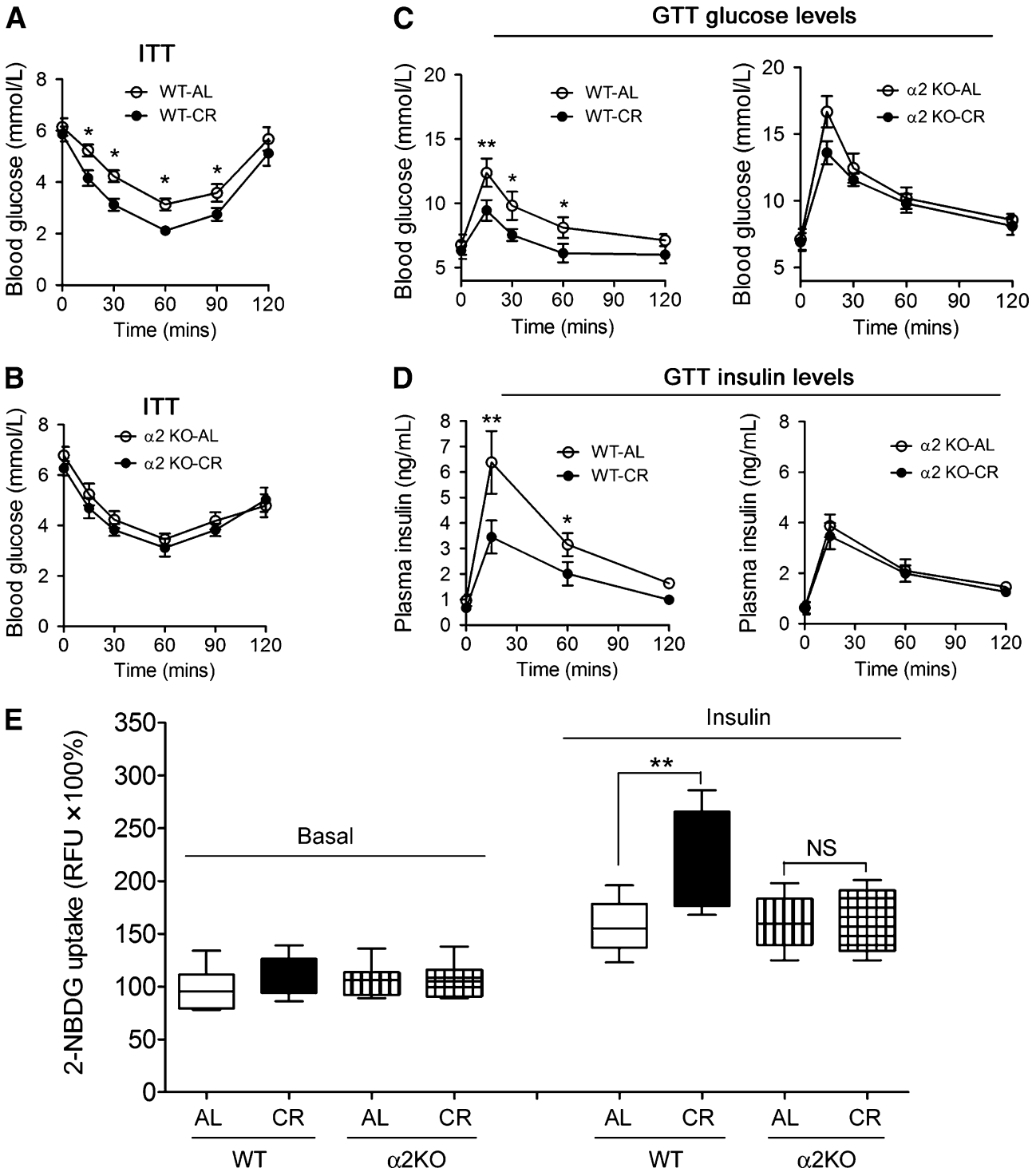

FIG. 2. Loss of AMPK-α2 impairs the CR-induced insulin-sensitizing effect and increase of glucose uptake in skeletal muscle. *A* and *B*: After 8 weeks of AL or CR treatment, ITT assay showing that CR improved insulin sensitivity in aged 16–17 week WT mice (*A*) but not in age-matched AMPK-α2 knockout (α2KO) mice (*B*). *C* and *D*: GTT assay showing the glucose (*C*) and insulin (*D*) levels of WT and AMPK-α2$^{-/-}$ mice. The insulin-sensitizing effect of CR was significantly reduced in AMPK-α2$^{-/-}$ mice. *E*: Loss of AMPK-α2 abolished the CR-induced increase of uptake of a fluorescent deoxyglucose analog (2-NBDG) in fresh isolated skeletal muscle. *P < 0.05, **P < 0.01 vs. AL. n = 8 per group. RFU, relative fluorescence units.

We further evaluated the phosphorylation of TBC1D1 and TBC1D4, two downstream targets of Akt and important regulators of insulin functions in skeletal muscle (28). CR increased phosphorylation of TBC1D1 (Fig. 3*C*) and TBC1D4 (Fig. 3*D*) upon insulin stimulation, which were reduced by deletion of AMPK-α2 (Fig. 3*C* and *D*).

Loss of AMPK-α2 counteracts the effects of CR on IRS-1 Ser phosphorylation through mTOR-S6K1 signaling pathway. Since it has been reported that Tyr phosphorylation of IRS-1 is positively regulated by phosphorylation of IR/IGF-IR (29), which was not altered by deletion of AMPK-α2 as shown above, and

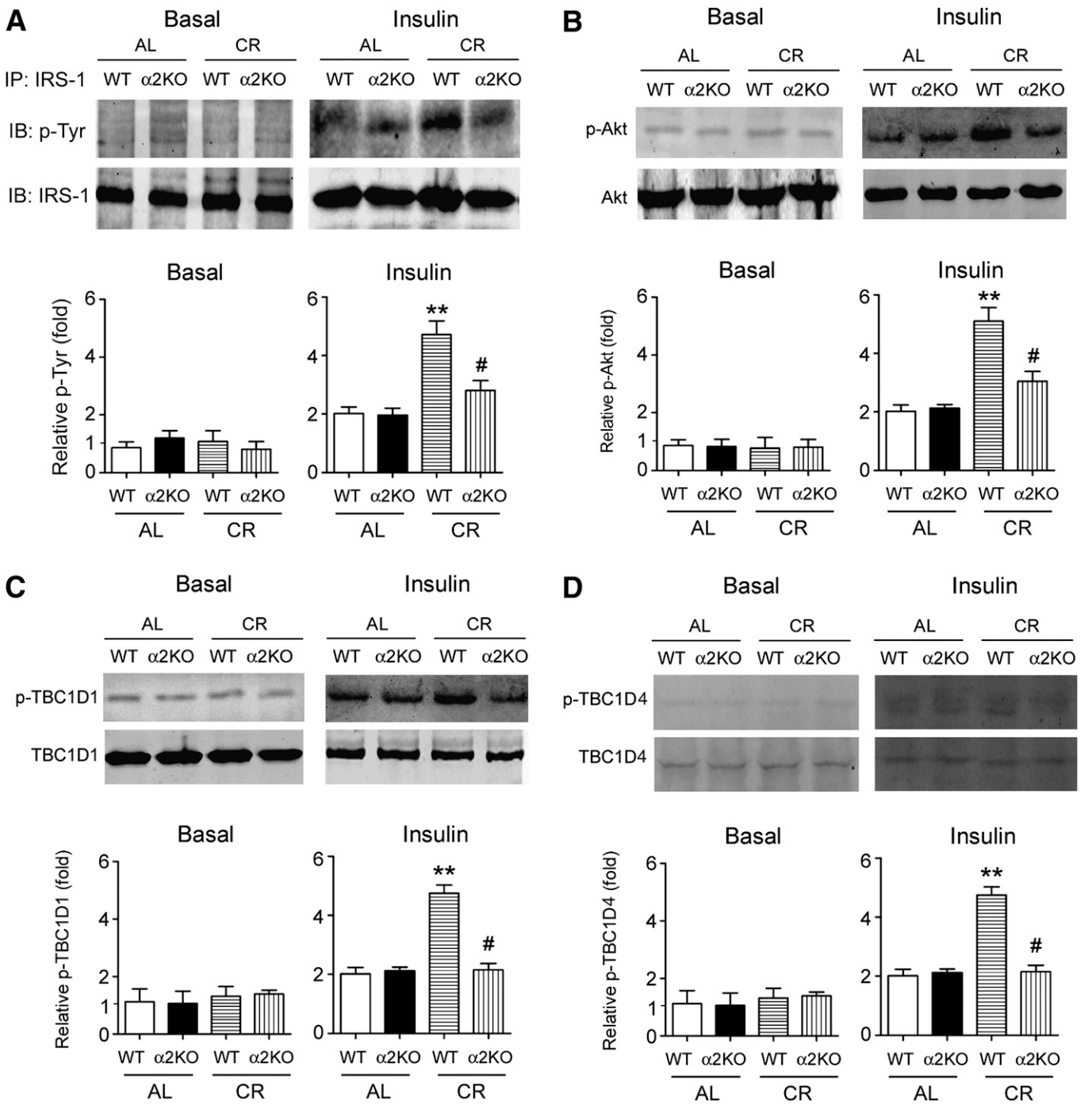

FIG. 3. Loss of AMPK-α2 hampers the CR-induced activation of the IRS-1–Akt signal pathway. *A*: IRS-1 was enriched by immunoprecipitation and then probed with anti–phospho-Tyr antibody to detect the Tyr phosphorylation in skeletal muscle of mice. *B–D*: In skeletal muscle of mice upon insulin stimulation, the influences of CR on phosphorylation of Akt (*B*), TBC1D1 (*C*), and TBC1D4 (*D*) were impaired by deletion of AMPK-α2. ***P* < 0.01 vs. WT-AL, #*P* < 0.05 vs. WT-CR. *n* = 4 per group. α2KO, AMPK-α2 knockout mice; IP, immunoprecipitation; IB, immunoblot.

negatively regulated by Ser phosphorylation of IRS-1 (29), we speculated that lack of AMPK-α2 could affect Tyr phosphorylation of IRS-1 by modulating Ser phosphorylation of IRS-1. Thus, we analyzed four Ser sites (Ser^{1101}, $Ser^{636/639}$, Ser^{612}, and Ser^{307}) of IRS-1. CR decreased phosphorylation of IRS-1 at Ser^{1101}, $Ser^{636/639}$, and Ser^{612} but not at Ser^{307} (Fig. 4*A* and *B*). Loss of AMPK-α2 abrogated the decline of IRS-1 phosphorylation at Ser^{1101} and $Ser^{636/639}$ but not at Ser^{612} (Fig. 4*A* and *B*), suggesting Ser^{1101} and $Ser^{636/639}$ could be modulated by AMPK-α2 upon CR.

Phosphorylation of IRS-1 at Ser^{1101} and $Ser^{636/639}$ has been reported to be regulated by the mTORC1-S6K1 pathway (30,31), while AMPK regulates phosphorylation of mTOR (11). We therefore examined the phosphorylation of the mTOR-S6K1 signal pathway. In WT mice, CR decreased the levels of phospho-S6K1, phospho-mTOR, and total mTOR (Fig. 4*C* and *D*). Such responses were absent in AMPK-$\alpha2^{-/-}$ mice (Fig. 4*C* and *D*).

Loss of AMPK-α2 compromises the effects of CR on the Nampt-SIRT1 cascade. We next tested whether the ablation of AMPK-α2 affects the SIRT1 activation upon CR

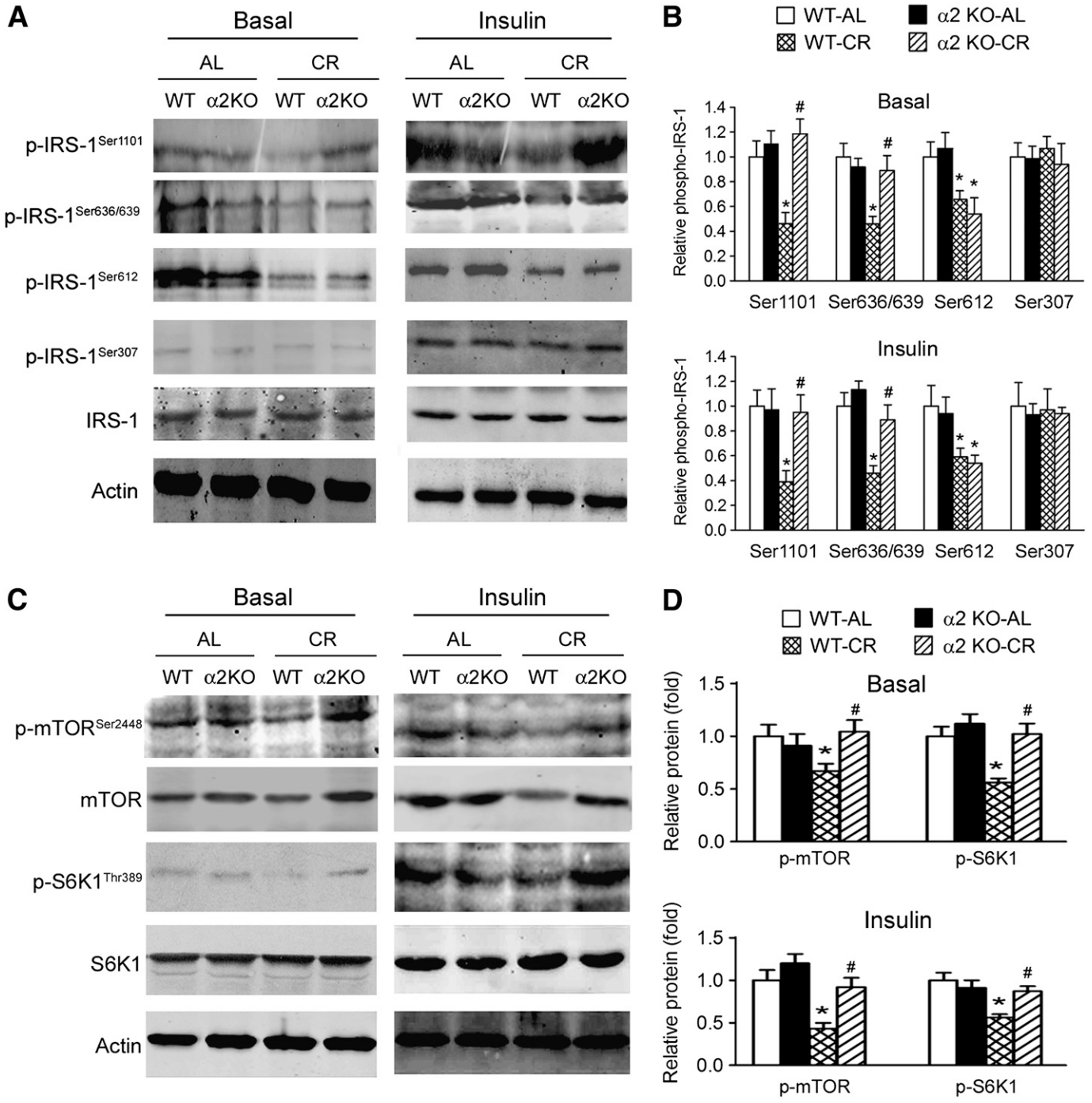

FIG. 4. Loss of AMPK-α2 impairs the CR-induced modulation of Ser phosphorylation of IRS-1 and the mTORC1-S6K1 signal pathway. *A* and *B*: Effects of CR on four Ser phosphorylation sites (Ser^{1101}, $Ser^{636/639}$, Ser^{612}, and Ser^{307}) of IRS-1 in skeletal muscle. The decreases of Ser^{1101} and $Ser^{636/639}$ phosphorylation of IRS-1 by CR were impaired in AMPK-$\alpha2^{-/-}$ mice. *C* and *D*: Effects of CR on phosphorylation of mTOR-S6K1 signal pathway were blocked by deletion of AMPK-α2. *$P < 0.05$ vs. WT-AL, #$P < 0.05$ vs. WT-CR. $n = 6$ per group. α2KO, AMPK-α2 knockout mice.

in skeletal muscle. CR increased SIRT1 protein level in both WT and AMPK-$\alpha2^{-/-}$ mice (Fig. 5*A*). However, the AMPK-$\alpha2^{-/-}$ mice exhibited less increase of SIRT1 activity upon CR (Fig. 5*B*). To further determine SIRT1 activity, we examined deacetylation of PGC-1α and FOXO1 by SIRT1. CR enhanced the deacetylation of PGC-1α and FOXO1 in WT mouse muscle and to a much lesser degree, in AMPK-$\alpha2^{-/-}$ mice (Fig. 5*C*).

Since SIRT1 activity is largely controlled by the NAD^+ level, which in turn is controlled by Nampt (32–34), we next studied the influences of deletion of AMPK-α2 on NAD^+ level and Nampt. As shown in Fig. 5*D*, CR increased the NAD concentration in WT control mice and to a much lesser degree, in AMPK-α2 knockout mice. Nampt protein expression was upregulated by CR in WT mouse muscle (Fig. 5*E*), which was partly suppressed in AMPK-$\alpha2^{-/-}$ mice (Fig. 5*E*).

CR upregulates AMPK-α2 though increasing protein stability of AMPK-α2. In line with the in vivo data, CR serum treatment increased the total AMPK-α2 and *p*-AMPK

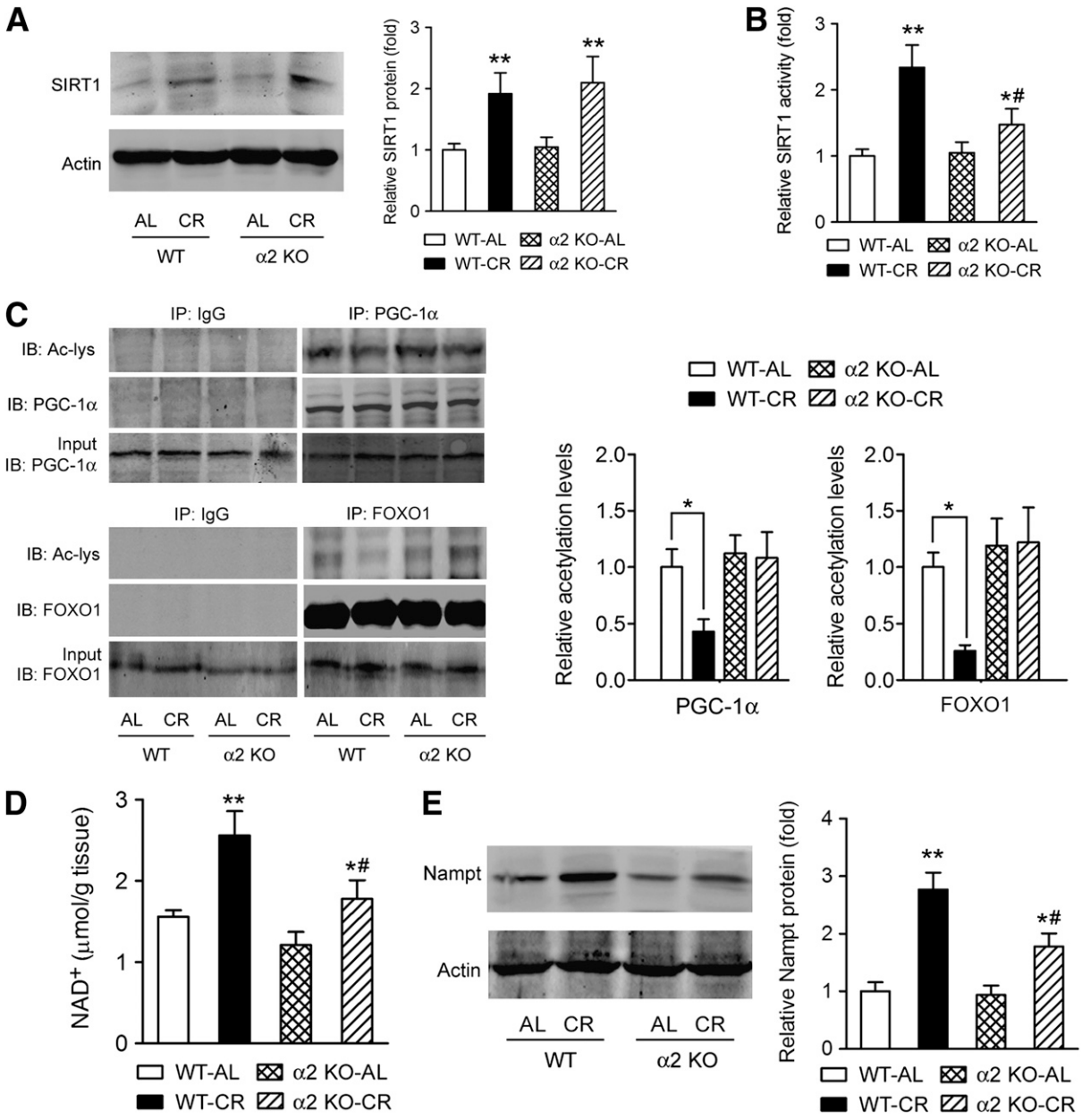

FIG. 5. Loss of AMPK-α2 compromises the CR-induced activation of Nampt-SIRT1 axis. *A*: The increase of SIRT1 protein expression by CR in muscle was not affected by loss of AMPK-α2. *B*: SIRT1 was enriched by immunoprecipitation and then subjected to an acetylation activity assay to determine the SIRT1 activity. The increase of SIRT1 activity in muscle of CR mice was blunted by deletion of AMPK-α2. *C*: PGC-1α and FOXO1 were immunoprecipitated and probed with anti–acetyl-Lys (Ac-Lys) to assess the acetylation of PGC-1α and FOXO1, which reflect the deacetylation ability of SIRT1. CR increased deacetylation of PGC-1α and FOXO1 in skeletal muscle in WT mice but not in AMPK-α2$^{-/-}$ mice. *D*: Effects of CR on the NAD$^+$ level in skeletal muscle were suppressed in AMPK-α2$^{-/-}$ mice. *E*: The upregulation of Nampt protein by CR was attenuated by deletion of AMPK-α2. *$P < 0.05$, **$P < 0.01$ vs. AL; #$P < 0.05$ vs. WT. $n = 6$ per group. α2 KO, AMPK-α2 knockout mice; IP, immunoprecipitation; IB, immunoblot.

levels in cultured C2C12 cells (Supplementary Fig. 3). However, the AMPK-α2 mRNA level of skeletal muscle was not affected by CR (Supplementary Fig. 4). This discrepancy suggests a likelihood of posttranslational regulation of AMPK-α2. First, we tested whether the increase in phospho-AMPK is due to changes in the upstream kinase of AMPK or the phosphatase of AMPK. CR serum did not affect phospho-LKB1 (Supplementary Fig. 5), the major upstream kinase of AMPK in skeletal muscle (35), or mRNA level and activity of PP2A and PP2C (Supplementary Fig. 6), two major phosphatases of AMPK (11), excluding the preceding possibilities.

Hence, we next examined whether CR affects AMPK-α2 protein stability. Treatment with MG132, a proteasome inhibitor, dramatically increased AMPK-α2 levels in C2C12 cells (Fig. 6*A*). Since polyubiquitylation can hamper the phosphorylation of AMPK and AMPK-related kinases (36), we tested whether CR could increase AMPK-α2 stability by modulating the ubiquitin-proteasome system. As shown in Fig. 6*B*, CR serum significantly decreased the amount of polyubiquitinated AMPK-α2 in C2C12 myotubes.

The protein stability of AMPK-α2 was evaluated by degradation curve of AMPK-α2 via blocking protein synthesis with CHX. The half-life of AMPK-α2 was increased significantly by

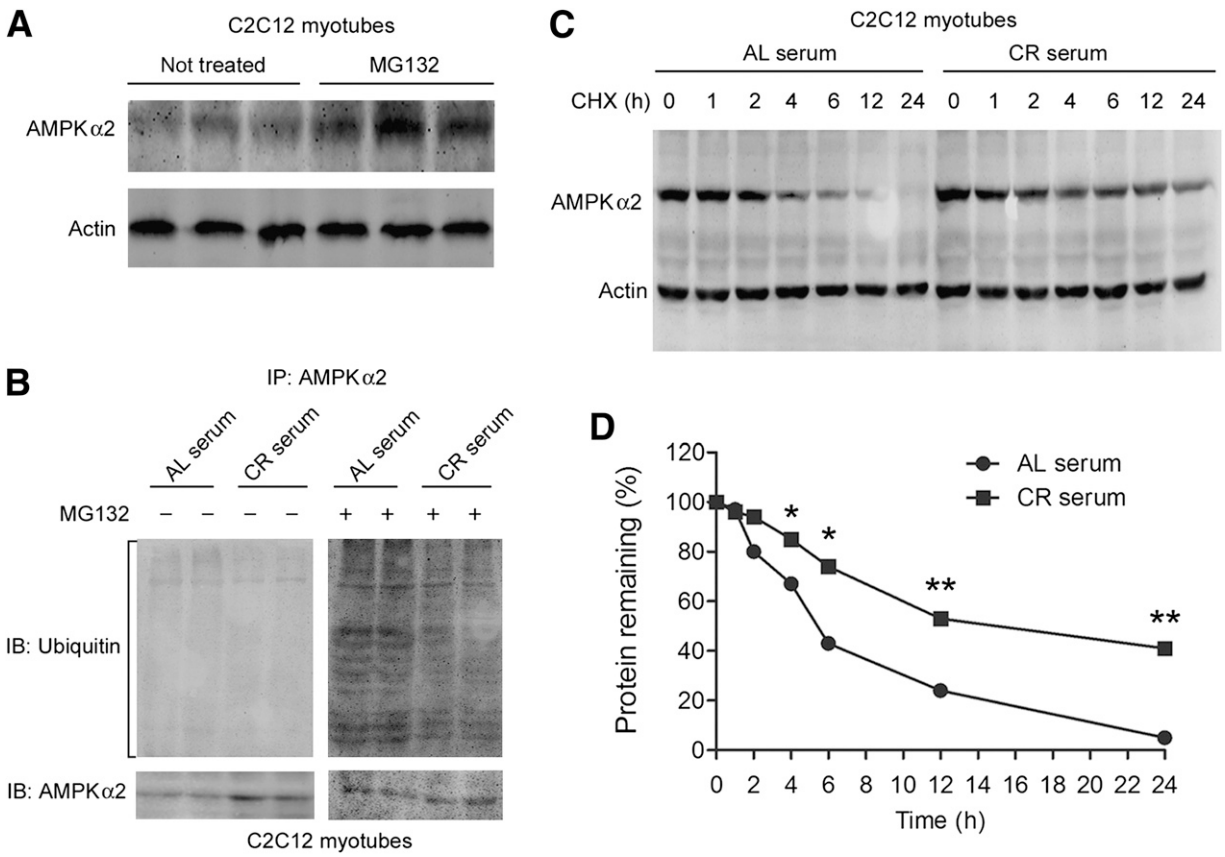

FIG. 6. CR increases AMPK-α2 protein stability by inhibiting ubiquitylation of AMPK-α2. *A*: C2C12 myoblasts were treated with the proteasome inhibitor MG132 (10 μmol/L) for 4 h before immunoblotting of AMPK-α2. *B*: C2C12 myotubes were serum starved and then incubated with serum from AL- or CR-treated C57BL/J6 mice (0.2 mL serum in 2 mL culture medium [10%]) for 8 h, and then the levels of polyubiquitinated AMPK-α2 were determined. *C*: C2C12 myotubes were serum starved and treated with 150 μg/mL CHX to block protein synthesis. Next, the cells were incubated with AL or CR serum (10%), and the degradation of AMPK-α2 protein level was determined. *$P < 0.05$, **$P < 0.01$ vs. AL serum. $n = 4$ per group. *D*: Degradation curve of AMPK-α2. IP, immunoprecipitation; IB, immunoblot.

CR serum (12–14 h vs. 4–6 h in AL serum-treated cells) (Fig. 6*C* and *D*), indicating that AMPK-α2 protein stability is increased by CR.

USP9X mediates the ubiquitylation-dependent degeneration of AMPK-α2. Knock down of USP9X, but not USP5 and USP7, with siRNA blocked the ubiquitylation-dependent degradation of AMPK-α2 (Fig. 7*A*). On the basis of all the data, we proposed a scheme for the critical role of AMPK-α2 in the regulation of the insulin-sensitizing effect of CR in skeletal muscle (Fig. 7*B*).

DISCUSSION

In this study, CR induced comparable body weight loss in WT and AMPK-α2$^{-/-}$ mice. Effects of CR on the fat pad weight, serum fasting glucose, serum triglycerides, serum NEFAs, and serum leptin levels were also comparable between WT and AMPK-α2$^{-/-}$ mice. However, the beneficial effects of CR on fasting/fed insulin and fed glucose levels existed only in WT mice, suggesting that deletion of AMPK-α2 could impair the insulin-sensitizing effects of CR. GTTs and ITTs confirmed that the insulin-sensitizing effects of CR were abolished in AMPK-α2$^{-/-}$ mice. These in vivo experiments were carried out in mice and may not necessarily reflect the situation in skeletal muscle. The next set of experiments was carried out in skeletal muscle isolated from AMPK-α2 knockout mice versus WT control mice. The results demonstrated that CR increases glucose uptake in WT control skeletal muscle but not in muscle isolated from AMPK-α2$^{-/-}$ mice. Skeletal muscle, adipose, and liver are thought to be classical insulin target tissues. Although there is no consensus on which tissue is most important for insulin action associated with CR, skeletal muscle is considered to account for much of the systemic action of insulin (37). Consequently, we concluded that loss of AMPK-α2 impairs the insulin-sensitizing effect of CR in skeletal muscle.

In the following mechanism study, we found that genetic ablation of the AMPK-α2 largely attenuated the increase of IRS-1 Tyr phosphorylation upon CR. The insulin−IR−IRS-1−Akt signaling pathway critically regulates glucose metabolism (38). In our study, deletion of AMPK-α2 did not modulate phosphorylation of IR/IGF-IR. The assay of screening of IRS-1 Ser phosphorylation sites showed that deficiency of AMPK-α2 impaired the decreases of IRS-1 phosphorylation at Ser$^{636/639}$ and Ser^{1101} induced by CR. The mTOR-S6K1 signaling pathway, which has been shown to enhance the IRS-1 phosphorylation at Ser$^{636/639}$ and Ser^{1101} (30,31,39), was also suppressed by CR in WT mice but not in AMPK-α2$^{-/-}$ mice. These data suggest that the disrupted inactivation of the mTOR-S6K1 signaling pathway contributes to the impaired insulin-sensitizing effects of CR in AMPK-α2$^{-/-}$ mice. The results also indicate that phosphorylation of IRS-1 may be more important than the

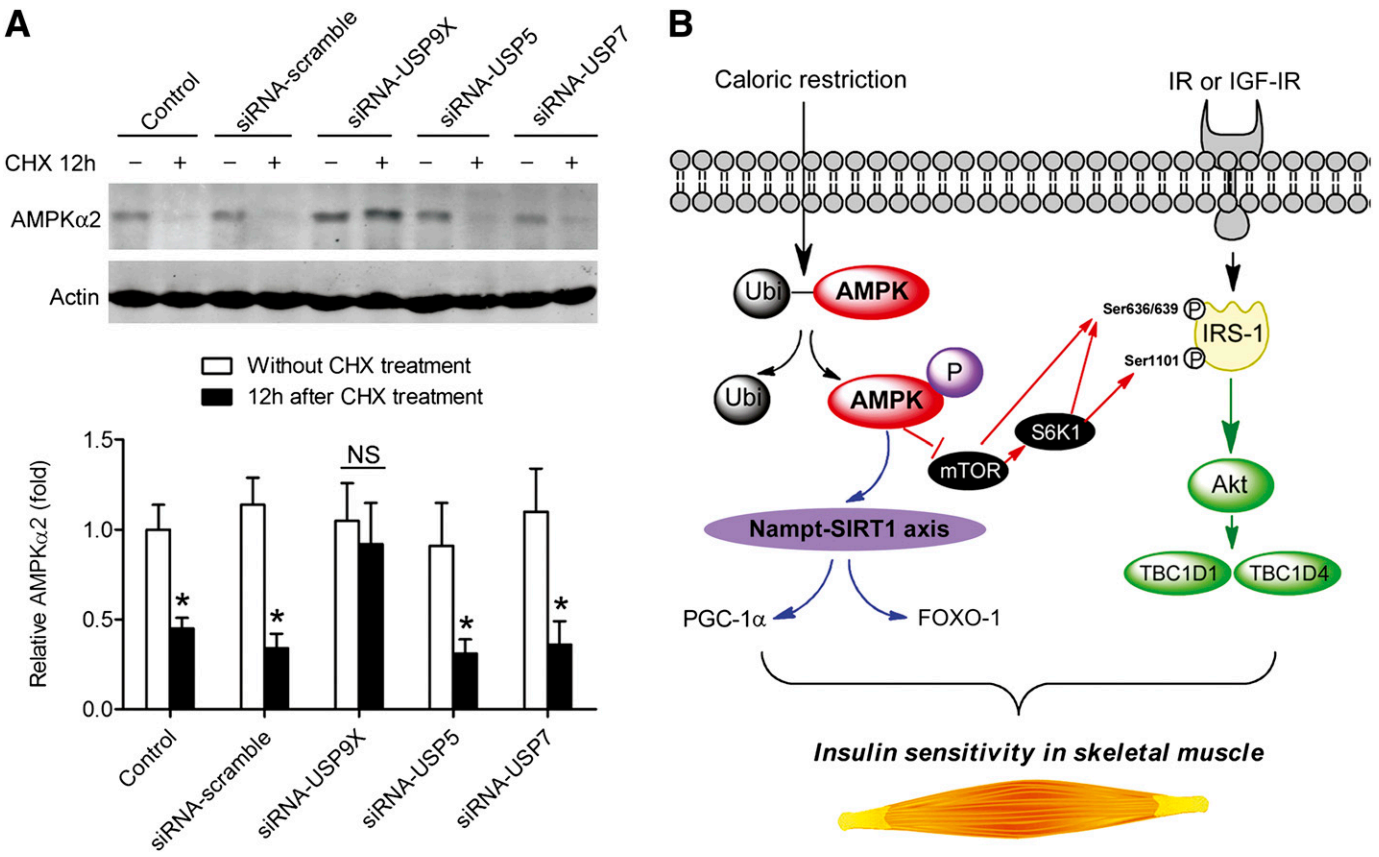

FIG. 7. Knock down of USP9X, but not USP5 and USP7, blocks the ubiquitylation-mediated degeneration of AMPK-α2. *A*: C2C12 myoblasts were transfected by siRNA-USP9X, siRNA-USP5, and siRNA-USP7 and then exposed to CHX for 12 h to block protein synthesis. AMPK-α2 protein levels in cells without and with CHX treatment (12 h) were determined by immunoblotting. Knock down of USP9X, but not USP5 and USP7, blocked the ubiquitylation-mediated degeneration of AMPK-α2. *$P < 0.05$ vs. without CHX treatment. *B*: Proposed scheme for the critical role of AMPK in the regulation of insulin-sensitizing effect of caloric restriction. AMPK-α2 plays a critical role in CR-induced insulin-sensitizing effect in skeletal muscle through regulating mTOR–S6K1–IRS-1 Ser phosphorylation and the Akt-TBC1D1/TBC1D4 signal pathway. AMPK-α2 is also required for the activation of the Nampt-NAD^+-SIRT1 axis in skeletal muscle during caloric restriction. Ubi, ubiquitylation.

phosphorylation of IR/IGF-IR for the enhancement of insulin sensitivity during CR. Together with the abolished induction of CR on Akt and TBC1D1/TBC1D4 in AMPK-$\alpha2^{-/-}$ mice, it is reasonable to conclude that the altered IRS-1 Ser phosphorylation is one of the key mechanisms by which CR regulates the IR–IRS-1–Akt signal pathway.

SIRT1 is widely believed to be mainly responsible for the benefits of CR (40). Recent studies indicate a critical role of AMPK in the extended life span induced by CR (41,42). We and others have previously demonstrated that Nampt is an important protector against various types of stress (20,43,44). Nampt has also been reported to be an important regulator in insulin secretion and glucose homeostasis (45). In this study, we demonstrated that AMPK activation by CR in the skeletal muscle precedes and determines the changes in Nampt expression, NAD^+ level, and SIRT1 activity. The compromised SIRT1 activity in AMPK-$\alpha2^{-/-}$ mice upon CR, in turn, abolished the CR-induced deacetylation of PGC-1α and FOXO1. Acetylation in the COOH-terminal region of the DNA binding domain of FOXO1 by p300 and cAMP-responsive element–binding protein and deacetylation by SIRTs greatly modulated FOXO regulatory function on glucose and lipid metabolism (46). In addition, reversible acetylation-deacetylation of PGC-1α is an important feature that contributes to the adaptation of mitochondrial energy homeostasis to changes in energy levels in insulin sensitivity regulation (47). These data suggest that under the CR condition, loss of AMPK-α2 effectively abrogates the increase of SIRT1 activity through inhibiting Nampt expression and NAD^+ level and thereby makes Nampt the possible link between AMPK and SIRT1.

Results from the in vitro experiments suggested that USP9X mediates the ubiquitin-dependent degradation of AMPK-α2. Ubiquitination is a posttranslational modification that can rapidly alter protein function via proteasome-mediated degradation. It has been reported that the major metabolic effect of insulin in muscle is inhibition of protein degradation via the ubiquitin-proteasome system (9). Our findings support the hypothesis that one of the contributing mechanisms underlying the insulin-sensitizing effect of CR is secondary to changes in the ubiquitin-proteasome system in skeletal muscle. Because polyubiquitylation of AMPK has been shown to hamper the phosphorylation of AMPK (36), the inhibited polyubiquitylation of AMPK-α2 in C2C12 cells by CR serum would help to enable more AMPK-α2 protein to be phosphorylated/activated. It should be noted that the phosphorylation of AMPK-α2 was increased upon CR even after correcting by total AMPK-α2, suggesting ubiquitylation-independent mechanisms also participated in increased phosphorylation of AMPK-α2 by CR.

AMPK-α2 null mice on an AL diet are reported to be insulin resistant because of alteration in sympathetic

nervous activity (16). Whether the existed insulin resistance contributes to the lessened response to CR in AMPK-$\alpha2^{-/-}$ mice is unknown, but the possibility exists. AMPK may influence the insulin-sensitizing effect of CR through both local and systemic action, which remains to be studied in the future. Also, the unknown serum factor(s) that mediate the CR-induced insulin-sensitizing action need to be identified in further studies.

In summary, we demonstrated that upregulation of AMPK-α2 is critical in the insulin-sensitizing effect of CR in skeletal muscle. We also showed that CR-induced AMPK-α2 upregulation in skeletal muscle is partly mediated by decreased polyubiquitylation of AMPK-α2. These data provide first evidence that the CR-induced insulin-sensitizing effect in skeletal muscle requires functional AMPK-α2 (Fig. 7*B*).

ACKNOWLEDGMENTS

This work was supported by grants from the National Natural Science Foundation of China (81100866 to P.W. and 81130061 to C.-Y.M.), the National Basic Research Program of China (2009CB521902 to C.-Y.M.), the Program of Shanghai Subject Chief Scientist (10XD1405300 to C.-Y.M.), the Shanghai 'Shu Guang' Project (10GG19 to C.-Y.M.), and the Second Military Medical University Young Investigator Foundation (2010QN06 to P.W.).

No potential conflicts of interest relevant to this article were reported.

P.W. researched data and wrote the manuscript. R.-Y.Z., J.S., Y.-F.G., T.-Y.X., and H.D. researched data and reviewed and edited the manuscript. B.V. discussed the study and reviewed the manuscript. C.-Y.M. designed the study and reviewed the manuscript. C.-Y.M. is the guarantor of this work and, as such, had full access to all the data in the study and takes responsibility for the integrity of the data and the accuracy of the data analysis.

REFERENCES

1. Colman RJ, Anderson RM, Johnson SC, et al. Caloric restriction delays disease onset and mortality in rhesus monkeys. Science 2009;325:201–204
2. Dessein PH, Shipton EA, Stanwix AE, Joffe BI, Ramokgadi J. Beneficial effects of weight loss associated with moderate calorie/carbohydrate restriction, and increased proportional intake of protein and unsaturated fat on serum urate and lipoprotein levels in gout: a pilot study. Ann Rheum Dis 2000;59:539–543
3. Kirk E, Reeds DN, Finck BN, Mayurranjan SM, Patterson BW, Klein S. Dietary fat and carbohydrates differentially alter insulin sensitivity during caloric restriction [corrected in: Gastroenterology 2009;137:393]. Gastroenterology 2009;136:1552–1560
4. Flachs P, Rühl R, Hensler M, et al. Synergistic induction of lipid catabolism and anti-inflammatory lipids in white fat of dietary obese mice in response to calorie restriction and n-3 fatty acids. Diabetologia 2011;54:2626–2638
5. Wing RR, Blair EH, Bononi P, Marcus MD, Watanabe R, Bergman RN. Caloric restriction per se is a significant factor in improvements in glycemic control and insulin sensitivity during weight loss in obese NIDDM patients. Diabetes Care 1994;17:30–36
6. Taguchi A, White MF. Insulin-like signaling, nutrient homeostasis, and life span. Annu Rev Physiol 2008;70:191–212
7. McCurdy CE, Cartee GD. Akt2 is essential for the full effect of calorie restriction on insulin-stimulated glucose uptake in skeletal muscle. Diabetes 2005;54:1349–1356
8. Fontana L, Weiss EP, Villareal DT, Klein S, Holloszy JO. Long-term effects of calorie or protein restriction on serum IGF-1 and IGFBP-3 concentration in humans. Aging Cell 2008;7:681–687
9. Wang ZQ, Floyd ZE, Qin J, et al. Modulation of skeletal muscle insulin signaling with chronic caloric restriction in cynomolgus monkeys. Diabetes 2009;58:1488–1498
10. McCurdy CE, Davidson RT, Cartee GD. Brief calorie restriction increases Akt2 phosphorylation in insulin-stimulated rat skeletal muscle. Am J Physiol Endocrinol Metab 2003;285:E693–E700
11. Hardie DG. AMP-activated/SNF1 protein kinases: conserved guardians of cellular energy. Nat Rev Mol Cell Biol 2007;8:774–785
12. Viollet B, Athea Y, Mounier R, et al. AMPK: Lessons from transgenic and knockout animals. Front Biosci 2009;14:19–44
13. Xiao B, Sanders MJ, Underwood E, et al. Structure of mammalian AMPK and its regulation by ADP. Nature 2011;472:230–233
14. Um JH, Park SJ, Kang H, et al. AMP-activated protein kinase-deficient mice are resistant to the metabolic effects of resveratrol. Diabetes 2010;59:554–563
15. Fujii N, Ho RC, Manabe Y, et al. Ablation of AMP-activated protein kinase alpha2 activity exacerbates insulin resistance induced by high-fat feeding of mice. Diabetes 2008;57:2958–2966
16. Viollet B, Andreelli F, Jørgensen SB, et al. The AMP-activated protein kinase alpha2 catalytic subunit controls whole-body insulin sensitivity. J Clin Invest 2003;111:91–98
17. Palacios OM, Carmona JJ, Michan S, et al. Diet and exercise signals regulate SIRT3 and activate AMPK and PGC-1alpha in skeletal muscle. Aging (Albany NY) 2009;1:771–783
18. Al-Regaiey KA, Masternak MM, Bonkowski MS, Panici JA, Kopchick JJ, Bartke A. Effects of caloric restriction and growth hormone resistance on insulin-related intermediates in the skeletal muscle. J Gerontol A Biol Sci Med Sci 2007;62:18–26
19. Cantó C, Auwerx J. Calorie restriction: is AMPK a key sensor and effector? Physiology (Bethesda) 2011;26:214–224
20. Wang P, Xu TY, Guan YF, et al. Nicotinamide phosphoribosyltransferase protects against ischemic stroke through SIRT1-dependent adenosine monophosphate-activated kinase pathway. Ann Neurol 2011;69:360–374
21. Min J, Kyung Kim Y, Cipriani PG, et al. Forward chemical genetic approach identifies new role for GAPDH in insulin signaling. Nat Chem Biol 2007;3:55–59
22. Zhong L, D'Urso A, Toiber D, et al. The histone deacetylase Sirt6 regulates glucose homeostasis via Hif1alpha. Cell 2010;140:280–293
23. Wang P, Xu TY, Guan YF, Su DF, Fan GR, Miao CY. Perivascular adipose tissue-derived visfatin is a vascular smooth muscle cell growth factor: role of nicotinamide mononucleotide. Cardiovasc Res 2009;81:370–380
24. Wang P, Yang FJ, Du H, et al. Involvement of leptin receptor long isoform (LepRb)-STAT3 signaling pathway in brain fat mass- and obesity-associated (FTO) downregulation during energy restriction. Mol Med 2011;17:523–532
25. Wang P, Guan YF, Du H, Zhai QW, Su DF, Miao CY. Induction of autophagy contributes to the neuroprotection of nicotinamide phosphoribosyltransferase in cerebral ischemia. Autophagy 2012;8:77–87
26. de Cabo R, Fürer-Galbán S, Anson RM, Gilman C, Gorospe M, Lane MA. An in vitro model of caloric restriction. Exp Gerontol 2003;38:631–639
27. Imig JD, Dimitropoulou C, Reddy DS, White RE, Falck JR. Afferent arteriolar dilation to 11, 12-EET analogs involves PP2A activity and Ca2+-activated K+ channels. Microcirculation 2008;15:137–150
28. An D, Toyoda T, Taylor EB, et al. TBC1D1 regulates insulin- and contraction-induced glucose transport in mouse skeletal muscle. Diabetes 2010;59:1358–1365
29. Taniguchi CM, Emanuelli B, Kahn CR. Critical nodes in signalling pathways: insights into insulin action. Nat Rev Mol Cell Biol 2006;7:85–96
30. Ozes ON, Akca H, Mayo LD, et al. A phosphatidylinositol 3-kinase/Akt/mTOR pathway mediates and PTEN antagonizes tumor necrosis factor inhibition of insulin signaling through insulin receptor substrate-1. Proc Natl Acad Sci U S A 2001;98:4640–4645
31. Tremblay F, Brûlé S, Hee Um S, et al. Identification of IRS-1 Ser-1101 as a target of S6K1 in nutrient- and obesity-induced insulin resistance. Proc Natl Acad Sci U S A 2007;104:14056–14061
32. Revollo JR, Grimm AA, Imai S. The NAD biosynthesis pathway mediated by nicotinamide phosphoribosyltransferase regulates Sir2 activity in mammalian cells. J Biol Chem 2004;279:50754–50763
33. Garten A, Petzold S, Körner A, Imai S, Kiess W. Nampt: linking NAD biology, metabolism and cancer. Trends Endocrinol Metab 2009;20:130–138
34. Ho C, van der Veer E, Akawi O, Pickering JG. SIRT1 markedly extends replicative lifespan if the NAD+ salvage pathway is enhanced. FEBS Lett 2009;583:3081–3085
35. Sakamoto K, McCarthy A, Smith D, et al. Deficiency of LKB1 in skeletal muscle prevents AMPK activation and glucose uptake during contraction. EMBO J 2005;24:1810–1820
36. Al-Hakim AK, Zagorska A, Chapman L, Deak M, Peggie M, Alessi DR. Control of AMPK-related kinases by USP9X and atypical Lys(29)/Lys(33)-linked polyubiquitin chains. Biochem J 2008;411:249–260
37. Bartke A. Insulin and aging. Cell Cycle 2008;7:3338–3343

38. Saltiel AR, Pessin JE. Insulin signaling pathways in time and space. Trends Cell Biol 2002;12:65–71
39. Tzatsos A, Kandror KV. Nutrients suppress phosphatidylinositol 3-kinase/Akt signaling via raptor-dependent mTOR-mediated insulin receptor substrate 1 phosphorylation. Mol Cell Biol 2006;26:63–76
40. Bordone L, Guarente L. Calorie restriction, SIRT1 and metabolism: understanding longevity. Nat Rev Mol Cell Biol 2005;6:298–305
41. Schulz TJ, Zarse K, Voigt A, Urban N, Birringer M, Ristow M. Glucose restriction extends Caenorhabditis elegans life span by inducing mitochondrial respiration and increasing oxidative stress. Cell Metab 2007;6:280–293
42. Greer EL, Dowlatshahi D, Banko MR, et al. An AMPK-FOXO pathway mediates longevity induced by a novel method of dietary restriction in C. elegans. Curr Biol 2007;17:1646–1656
43. Yang H, Yang T, Baur JA, et al. Nutrient-sensitive mitochondrial NAD+ levels dictate cell survival. Cell 2007;130:1095–1107
44. Rongvaux A, Galli M, Denanglaire S, et al. Nicotinamide phosphoribosyl transferase/pre-B cell colony-enhancing factor/visfatin is required for lymphocyte development and cellular resistance to genotoxic stress. J Immunol 2008;181:4685–4695
45. Revollo JR, Körner A, Mills KF, et al. Nampt/PBEF/Visfatin regulates insulin secretion in beta cells as a systemic NAD biosynthetic enzyme. Cell Metab 2007;6:363–375
46. Barthel A, Schmoll D, Unterman TG. FoxO proteins in insulin action and metabolism. Trends Endocrinol Metab 2005;16:183–189
47. Jeninga EH, Schoonjans K, Auwerx J. Reversible acetylation of PGC-1: connecting energy sensors and effectors to guarantee metabolic flexibility. Oncogene 2010;29:4617–4624